Optical Properties of Europium and Terbium doped Lanthanum based Compounds

[1]Harshad Trivedi, [2]Ronak Patel, [3]Nidhishree M Suchak, [3*]M P Deshpande, [4]Kevil Shah, [4*]B S Chakrabarty,[1*]Vimal Joshi

[1,1*]Department of Physics, Shri R. K. Parikh Arts and Science College, Petlad.
[2]Department of Chemistry, Sardar Patel University, Anand.
[3,3*]Department of Physics, Sardar Patel University, Anand.
[4,4*]Department of Applied Physics, M.S. University, Vadodara.

Email. tharshad98@gmail.com

Abstract

Samples of Lanthanum Oxide (La_2O_3), Lanthanum Oxysulphide (La_2O_2S) and Lanthanum Phosphate ($LaPO_4$) activated by Europium (Eu) and Terbium (Tb) in different concentrations were prepared using Solid state synthesis method. They were characterized by X ray diffraction. The UV–Visible characteristics of the samples were investigated using UV–Visible spectrophotometer and the band gap of the samples was obtained by deriving a plot based on the Tauc relation. The UV absorption was found to be in the increasing order with concentration of the activators (1% to 4%). The samples doped with 2 mol % of the activators were considered for the study of luminescence characteristics, as 2 mol % is a common and reliable doping percentage. The emission spectra gave characteristic lines for Eu^{3+} and Tb^{3+} in the orange-red and blue-green region respectively.

Key Words: Lanthanum, Europium (Eu) and Terbium (Tb)

1 Introduction

Rare earth materials, particularly lanthanides, possess unique optical properties stemming from their 4f electron configurations, enabling efficient luminescence, sharp absorption, and lasing. [1,2] They enable tailored luminescence, sharp spectral emission from UV to near-infrared (NIR), long lifetimes, and high-index refraction. Key uses include phosphors, laser media and fiber-optic amplifiers. Rare earth (RE) compounds are uniquely suited for optical applications due to the localized electronic structure of their 4f orbitals, which remain shielded from surrounding host materials. This shielding results in atomic-like, sharp optical transitions with high quantum efficiency, allowing for the precise manipulation of light. Rare earth elements (Lanthanides) have partially filled 4f inner shells. Unlike transition metals, these 4f electrons are shielded by outer 5s and 5p electron shells. Because the 4f orbitals are shielded, the energy levels are relatively unaffected by the surrounding crystal field of the crystal lattice, similar to free atoms. [3] This results in sharp, monochromatic emission/absorption lines rather than broad bands. The shielding enables

some active rare earth ions to emit at specific, consistent wavelengths regardless of whether they are in a glass or crystal host. Energy can be efficiently transferred between different RE ions in co-doped materials, increasing the efficiency of pumping and photon emission. Among the rare earths, the compounds that act as good host matrices for optical applications are those of Lanthanum, Cerium, Gadolinium and Yttrium. These compounds include aluminates, oxides, phosphates and sulphides. [4,5] Lanthanum and Cerium are the lowest priced. However, Lanthanum compounds have more applications and find higher number of uses, particularly in luminescence applications. Erbium, Neodymium, Ytterbium and Holmium are good activating/co-activating ions for lasing and up-conversion materials. Cerium, Dysprosium, Europium and Terbium act as the down-conversion ions to convert UV into visible, thus making them ideal for luminescence applications. While Cerium and Dysprosium emit in relatively broad region.[6] Europium and Terbium have sharp emission peaks in the red and green region respectively. Sharp emission features provide better colour rendition properties in luminescent materials. Hence, compounds of Lanthanum namely Lanthanum Oxide (La_2O_3), Lanthanum Oxysulphide (La_2O_2S) and Lanthanum Phosphate ($LaPO_4$) were chosen as the host materials for the study along with Europium and Terbium as activators. While studies on Lanthanum Oxysulphide and Lanthanum Phosphate as luminescent materials are limited, Lanthanum Oxide is studied more. The inclusion of Lanthanum Oxide serves as a reference for comparison as well as validation for the method of synthesis and the luminescence characteristics.

2 Experimental

Eight samples were synthesized for each host [Lanthanum Oxide (La_2O_3), Lanthanum Oxysulphide (La_2O_2S) and Lanthanum Phosphate ($LaPO_4$)], four with Europium (Eu^{3+}) and four with Terbium (Tb^{3+}) as activator in increasing concentration of 1% (molar) to 4 % (molar) by Solid state synthesis method. Stoichiometric amounts of precursors were taken based on the required doping concentration by accurately weighing them on the analytical balance. The precursor powders were put in an agate mortar and pestle to grind them uniformly. Ethanol in appropriate quantity was used to turn it into a homogenous mixture paste. The process involved around an hour of grinding and mixing, as homogeneity aids in improved reactivity of the precursors.

In order to remove the ethanol, moisture and other residual solvents, the mixture paste was dried in a hot air oven at 150 °C for 4 hours. Small chunks were formed on drying. They were crushed and grinded again. The resulting powders for samples with different dopant concentrations were put in alumina crucibles for heating at high temperature to enable the solid-state reaction. These crucibles were transferred in a programmable muffle furnace for them to be heated at 1100 °C for 4 hours. It took several hours for the furnace to reach 1100 °C, after which it was held for 4 hours. After holding at 1100 °C, the furnace was allowed to cool naturally for 48 hours, for it to reach room temperature. The resulting product was a hard

chunk inside the crucibles. These chunks were carefully taken out from the crucibles into an agate mortar and pastel to be ground again to obtain a fine, uniform powder.

X-ray powder diffractograms were recorded on a Rigaku, Japan make Miniflex model X-ray diffractometer. All diffraction patterns were obtained using Cu K_α radiation (λ = 1.54051 A°), at 30 kV and 15 mA. Measurements were taken in the pertinent 2θ ranges varying between 10° and 70° with steps of 0.02°. The d- values from X ray diffraction pattern matched with the standard JCPDS database.

The UV–Visible characteristics of the samples (Eu^{3+} and Tb^{3+}doped La_2O_3, La_2O_2S and $LaPO_4$) were investigated using a TCC-240 Shimadzu make UV–Visible spectrophotometer. Equal amount of solute i. e. sample (3mg) was taken and dissolved in the same amount of solvent (10 mL) for each measurement. Tauc's plot was used for the calculation of optical band gap.

The samples were investigated for emission at an initial excitation wavelength of 254 nm on Perkin Elmer LS 55 Fluorescence Spectrometer. The deep ultraviolet 254 nm line was considered as it is the excitation wavelength of low-pressure mercury lamps like the common tube light. The integrator apparatus was needed to measure the Quantum Efficiency or Quantum Yield of the samples. The Horiba Yvon Fluoromax 4 system, apart from having the same features as the Perkin Elmer system, has the additional capability to measure the Quantum Yield. Hence, the spectra were re-recorded on this system. In an attempt to address the problem of low emission intensity, the samples were annealed at 800 C to remove any residual moisture and consolidating the bulk phase further. The annealed samples gave higher emission intensity with multiple peaks.

3 Results and Discussion

The UV–Visible characteristics of 24 samples, 4 different concentrations each of $Eu^{3+}$and Tb^{3+} in Lanthanum Oxide (La_2O_3), Lanthanum Oxysulphide (La_2O_2S) and Lanthanum Phosphate ($LaPO_4$) were recorded. The absorption curve along with the corresponding Tauc's plot of an illustrative sample is given below.

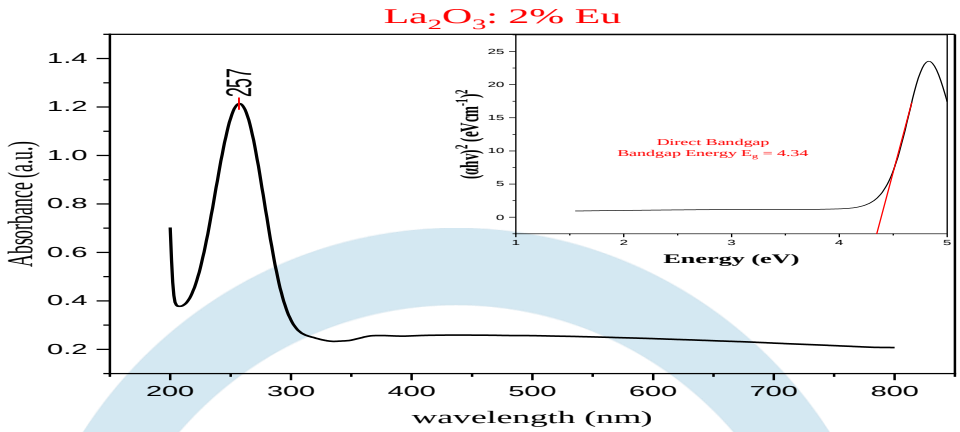

Fig.1: Absorption Spectra and Tauc's Plot for La_2O_3:2%Eu^{3+}

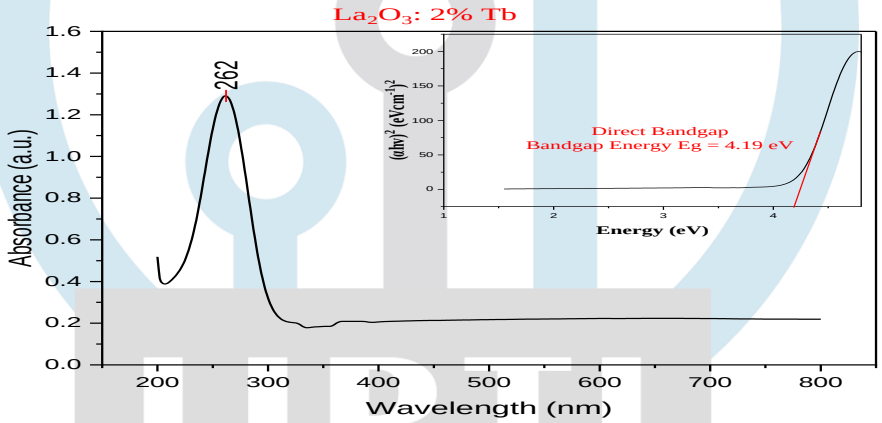

Fig.2: Absorption Spectra and Tauc's Plot for La_2O_3:2%Tb^{3+}

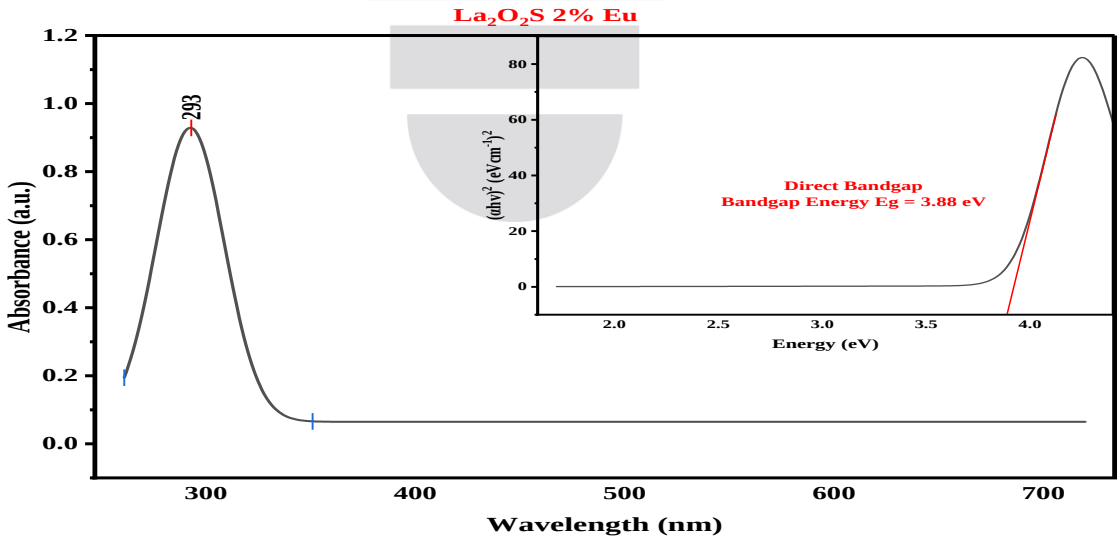

Fig.3: Absorption Spectra and Tauc's Plot for La_2O_2S:2%Eu^{3+}

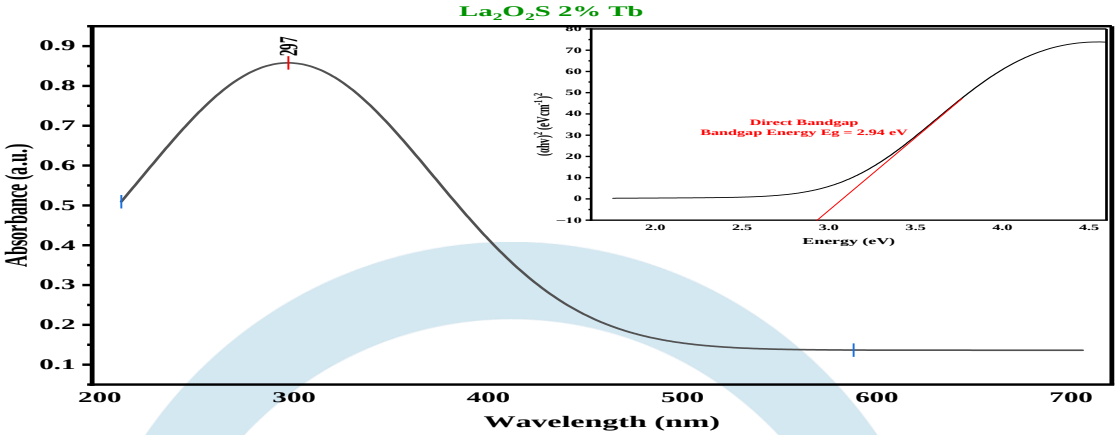

Fig.4: Absorption Spectra and Tauc's Plot for La_2O_2S:2%Tb^{3+}

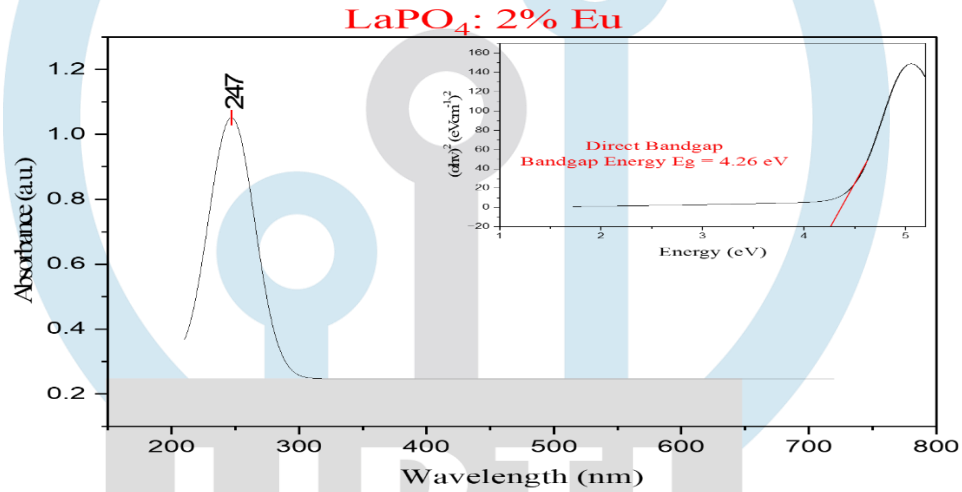

Fig.5: Absorption Spectra and Tauc's Plot for $LaPO_4$:2%Eu^{3+}

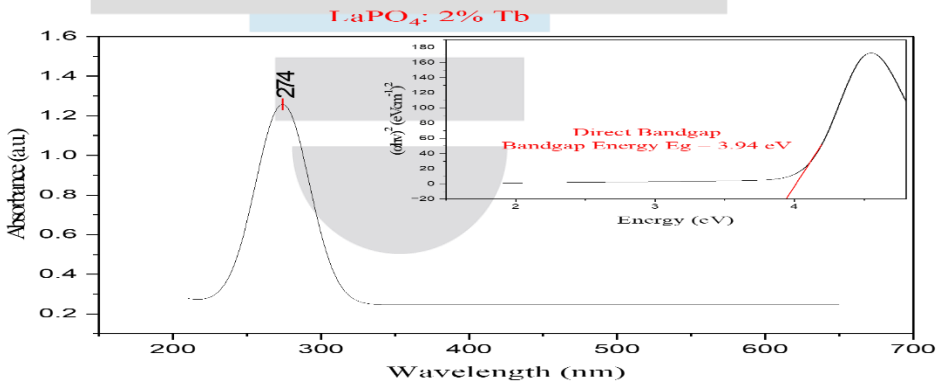

Fig.6: Absorption Spectra and Tauc's Plot for $LaPO_4$:2%Tb^{3+}

Table 1 consolidates the peak wavelength for maximum absorbance; the optical bandgap derived from the curves and the refractive index of all the samples.

No.	Compound		Absorption	Optical Bandgap	Refractive Index
			nm	eV	
1	La_2O_3	1% Eu	257	4.23	2.12
2		2% Eu	257	4.34	2.10
3		3% Eu	257	4.26	2.11
4		4% Eu	257	4.28	2.11
5		1% Tb	262	4.16	2.13
6		2% Tb	262	4.19	2.12
7		3% Tb	262	4.18	2.12
8		4% Tb	263	4.21	2.12
9	La_2O_2S	1% Eu	293	3.9	2.17
10		2% Eu	293	3.88	2.17
11		3% Eu	293	3.88	2.17
12		4% Eu	293	3.88	2.17
13		1% Tb	297	2.98	2.37
14		2% Tb	297	2.94	2.38
15		3% Tb	297	2.92	2.38
16		4% Tb	297	2.92	2.38
17	$LaPO_4$	1% Eu	247	4.29	2.11
18		2% Eu	247	4.26	2.11
19		3% Eu	245	4.31	2.10
20		4% Eu	245	4.32	2.10
21		1% Tb	274	3.95	2.16
22		2% Tb	274	3.94	2.16
23		3% Tb	274	3.92	2.17
24		4% Tb	274	3.94	2.16

Table 1: Values of Peak Absorption, Optical Bandgap and Refractive Index.

The absorption peaks of the samples were found to be at in a narrow range of wavelengths between **257 nm to 297 nm**. The Europium doped samples absorbed at lower wavelengths compared to Terbium doped samples, for the same host matrix. The Lanthanum based matrices are known to absorb in relatively deeper UV region. All samples showed strong absorption in the UV region. The absorption may involve the host as well as dopants. Apart from host absorption, direct transfer of energy to the dopant ions is also probable. Hence, the absorption energy can vary from dopant to dopant. [7,8,9]

The difference in peak wavelength for Eu and Tb doped samples is the minimum in La_2O_2S (4 nm) followed by La_2O_3 (6 nm) and $LaPO_4$ (29 nm). This suggests that there is minimal role of dopants in the absorption of UV in La_2O_3. This oxide of Lanthanum is the most stable matrix due to thermodynamic, geochemical and electrochemical factors. Phosphate of Lanthanum is also relatively stable. [10] Lanthanum phosphate exhibits high thermal stability and low solubility, contributing to its durability in materials applications.[11] The monoclinic phase of lanthanum phosphate ($LaPO_4$) is thermodynamically more stable, as indicated by its lower formation energy and favorable electronic structure.[12] However, Sulphides are the least stable in the presence of Oxygen. This also reflects on the spectroscopic properties of the host material and hence their optical absorption characteristics. Dopants also affect the optical absorption on account of the introduction of impurity levels.

The optical absorption mechanism in Rare Earth-doped Lanthanum based matrices is primarily driven by three distinct electronic processes:[13]

- host-to-dopant charge transfer
- intra-configurational transitions within the dopant ion
- band-to-band transitions of the host matrix

The host-to-dopant charge transfer also called Ligand-to-Metal Charge Transfer (LMCT) results in multiplicity of energy states, commonly referred to as Charge Transfer Band (CTB).[7]Charge transfer bands in rare-earth doped materials are attributed to ligand-to-metal charge transfer transitions involving electron transfer from surrounding anions to the dopant ion.[9]At high energies (typically below 230 nm), photons are absorbed by the host itself, exciting electrons from the valence band to the conduction band. Hence, the most prominent feature of this band is that the absorption spectrum is typically centered in the deeper ultraviolet region. [7,14] This involves an electronic transition from the orbital of the surrounding Oxygen ligands to the orbital of the trivalent dopant ion. Beinga parity-allowed transition, it is much stronger than the direct excitation of the ion itself. It efficient absorbs high-energy photons and transfers that energy to the dopant ions. [8,9] However, doping with often causes a slight redshift in the absorption edge due to the introduction of new energy states. The absorption, more specifically, is on account of transitions between the $\mathbf{4f^8}$ **and** $\mathbf{4f^75d}$ orbitals and charge transfer between $\mathbf{O^{2-}}$ / $\mathbf{S^{2-}}$ and the $\mathbf{X^{+3}}$ (dopant ion).[15]

The intra-configurational transitions within the dopant ion also called the Intra-4f transitions results in absorption in the longer UV and visible ranges (300–500 nm).[16] The absorption occurs via sharp, narrow lines corresponding to electronic transitions from $^7F_0 \rightarrow {}^5L_6$. They appear as sharp, discrete absorption lines in the UV and visible regions (typically 350–500 nm), corresponding to transitions from the

ground state to various excited states. Being forbidden by Laporte rules, this absorption has low intensity. [17,18]

The Host Band-to-Band Absorption, typically seen in wide-bandgap semiconductors occur at high energies (typically below 230 nm). Here, the photons are absorbed by the host itself, exciting electrons from the valence band to the conduction band. [19,20]

Apart from the above three, there can be Defect-Mediated Absorption due to the presence of oxygen vacancies and lattice distortions (often caused by the ionic size mismatch between host and dopant. These defects contribute to the Urbach energy and can cause broad, low-intensity absorption tails in the UV region. Hence, the absorption in all three systems is primarily due to the presence of a charge transfer band, which occurs due to the electronic transition between the 2p orbital energy levels of Oxygen and 4f/5d energy levels of the rare earth or dopant ion. [9,21,22]

The absorption values correspond to a bandgap range of **2.92 eV to 4.34 eV**. Absorption of the Europium doped samples being in deeper UV region, the bandgap values were on the higher side, averaging at **4.15 eV.** The Terbium doped samples have an average bandgap value of **3.68**. The lower value is due to the La_2O_2S samples, which averaged at 2.94 eV. The known bandgap values of La_2O_3 range from 4.3 to 5.5 eV, La_2O_2S from 2.1 to 4.0 eV and $LaPO_4$ from 3.9 to 4.5 eV. Hence, these values are consistent with the known bandgap values, although on the lower side of the range, which can be attributed to doping. Dopants do affect the optical absorption on account of the introduction of impurity levels or inducing structural defects, thus modifying the bandgap.[23]

A slight change in bandgap was observed with change in dopant concentration. However, it was random and did not give any particular trend. The band gap values are derived from the intercept of the line drawn from the linear region of the Tauc's plot on the energy axis. Hence, small variations are inherent in the process. Some electronic states are generated due to the dopant ions. This can result into band tailing on account of the extension of energy levels due to these electronic states, from the valence or conduction bands into the forbidden bandgap, forming tails of states, thus affecting the linearity of the extended region of the Tauc Plot and consequently, the bandgap values. [21,22,24]

Lanthanum based compounds generally display a wide optical and several parameters including doping can modify this band gap, which can be used to tailor the band gap for use in optoelectronic devices.

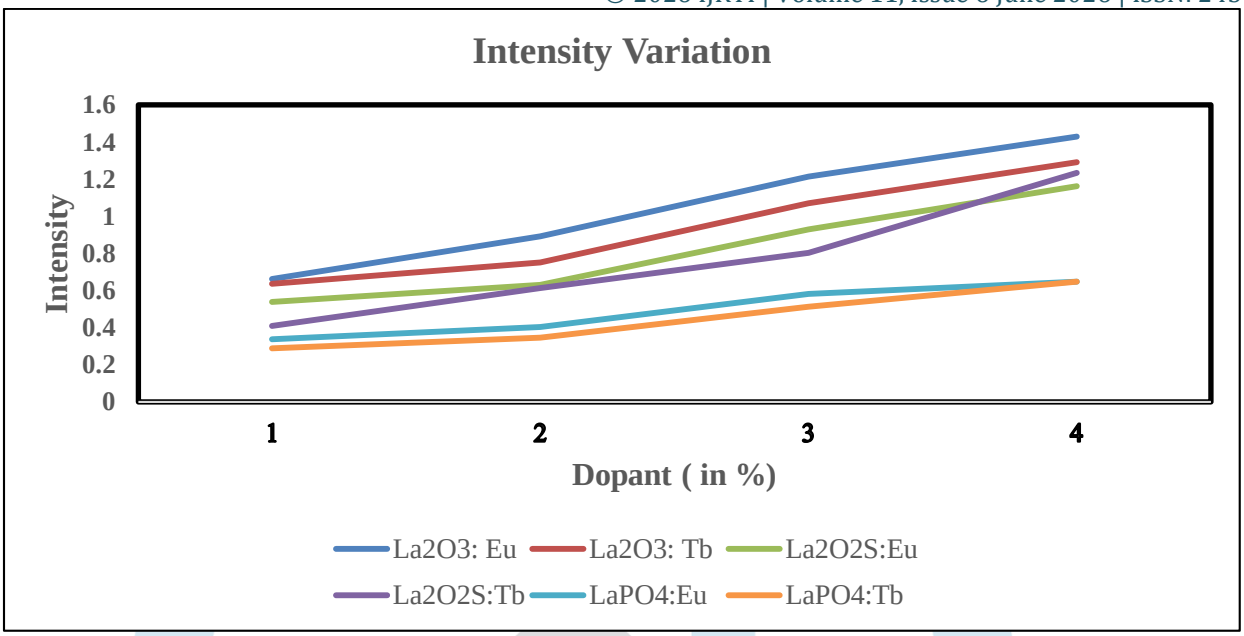

Fig. 7: Variation in the intensity of Dopant

The samples exhibit a pattern of variation in peak intensity with variation in the concentration of the dopants. The intensity increases with concentration. However, the variation is not strictly linear. The synthesis method of the samples has scope for non-uniform mixing of the dopant and host material, which may affect the incorporation of dopant ions in the host matrix, leading to non-uniform optical absorption [25,26]

The refractive index values of the Eu^{3+} and Tb^{3+} doped samples in La_2O_3, La_2O_2S, and $LaPO_4$ systems varied depending on the dopant concentration and host material. For the La_2O_3 system, the refractive index ranged from 2.10 to 2.12 for Eu^{3+} doping (1% to 4%) and 2.12 to 2.13 for Tb^{3+} doping, indicating minimal variation with change in dopant concentration. In the La_2O_2S system, the refractive index was higher with a value of 2.17 for Eu doped samples, and the highest value of 2.38 for Tb doped samples. Notably, the $LaPO_4$ system exhibited refractive index values on the same lines as La_2O_3, with around 2.10 for Eu doped samples and 2.16 for Tb doped samples.

Overall, the refractive index values suggest that dopant concentration and host matrix both influence optical density, but the changes are relatively subtle, likely due to the stable crystal field environments in the rare-earth host lattices. The samples doped with 2 mol % of the activators were considered for the study of luminescence characteristics, as 2 mol % is a common and reliable doping percentage.

The samples investigated for emission at an excitation wavelength of 254 nm on Perkin Elmer LS 55 Fluorescence Spectrometer gave emission at the standard lines of Eu^{3+} and Tb^{3+} around 590 nm and 540 nm respectively. However, the intensity of the emission peaks was very subdued. Besides, an integrator

apparatus was needed to measure the Quantum Efficiency or Quantum Yield of the samples. The Horiba Yvon Fluoromax 4 system, apart from having the same features as the Perkin Elmer system, has the additional capability to measure the Quantum Yield. Hence, the spectra were re-recorded on this system. In an attempt to address the problem of low emission intensity, the samples were annealed at 800 C to remove any residual moisture and consolidating the bulk phase further. The annealed samples gave higher emission intensity with multiple peaks. An illustrative sample of the excitation and emission peaks is given below.

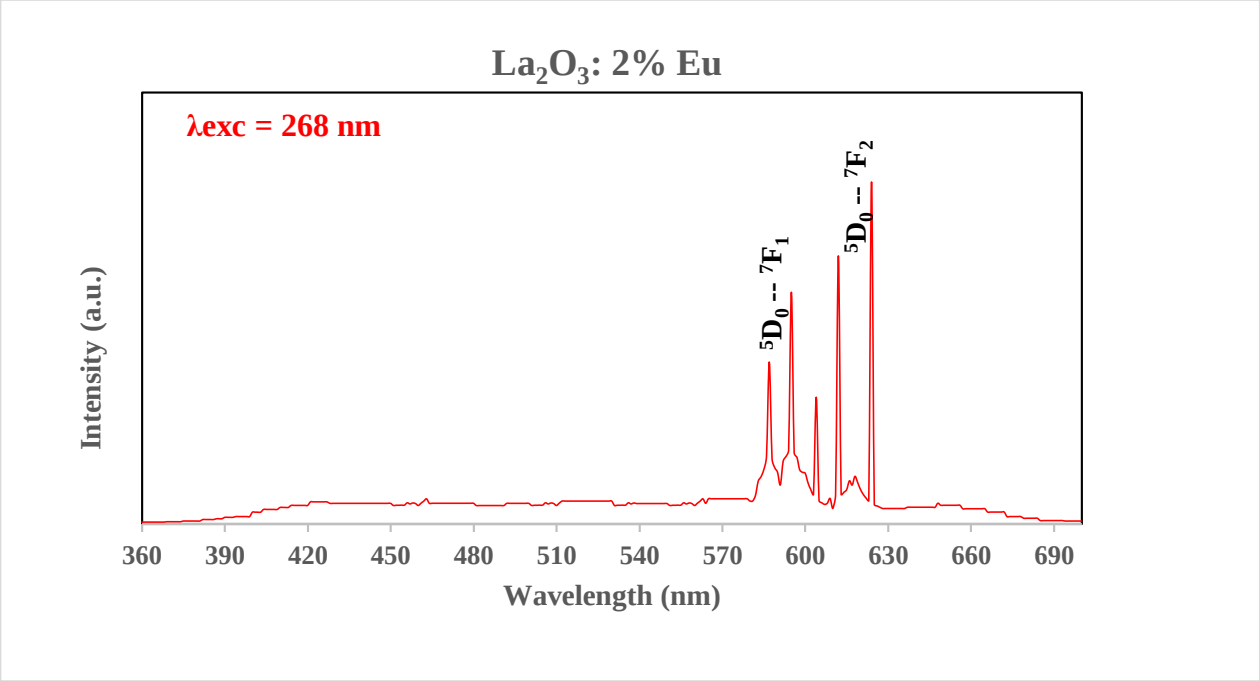

Fig.8: Emission spectra of La_2O_3:Eu^{3+}

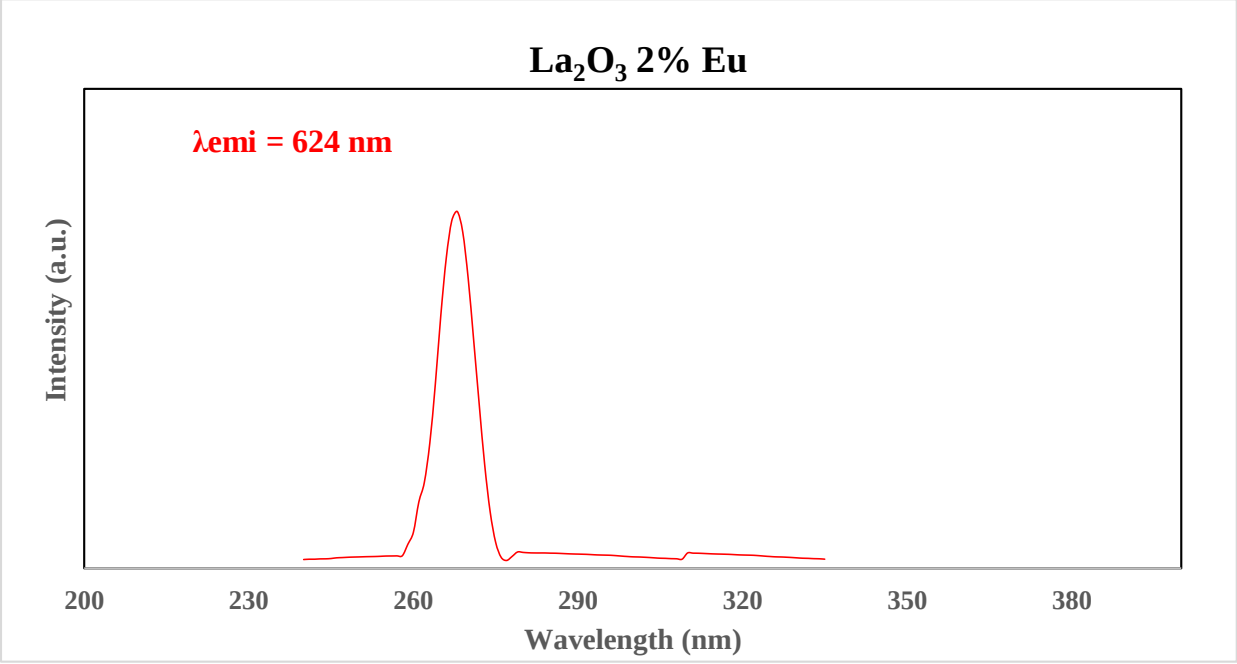

Fig.9: Excitation spectra of La_2O_3:Eu^{3+}

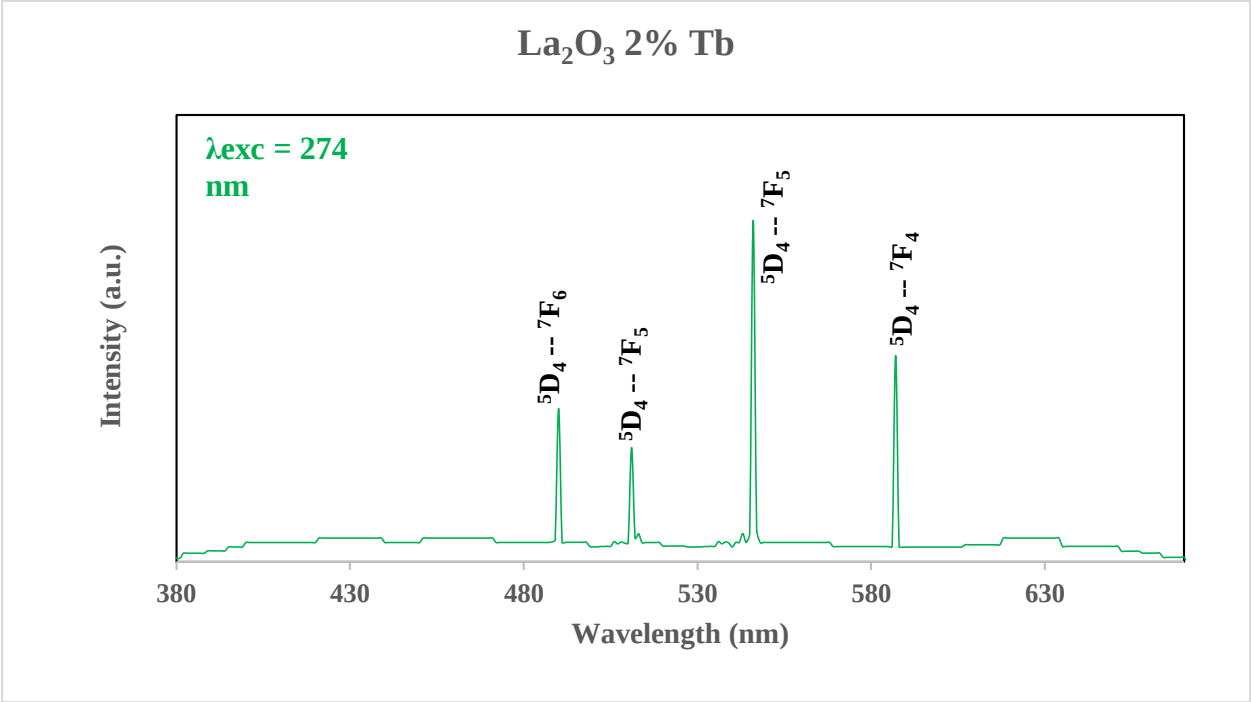

Fig. 10: Emission spectra of $La_2O_3:Tb^{3+}$

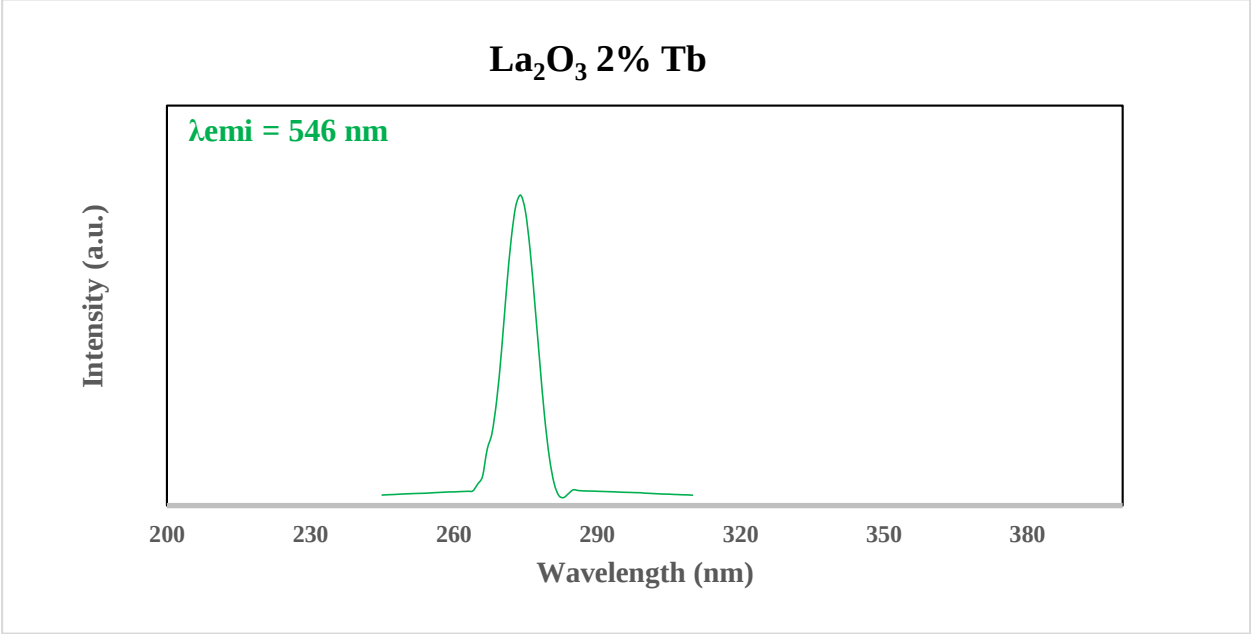

Fig. 12: Excitation spectra of $La_2O_3:Tb^{3+}$

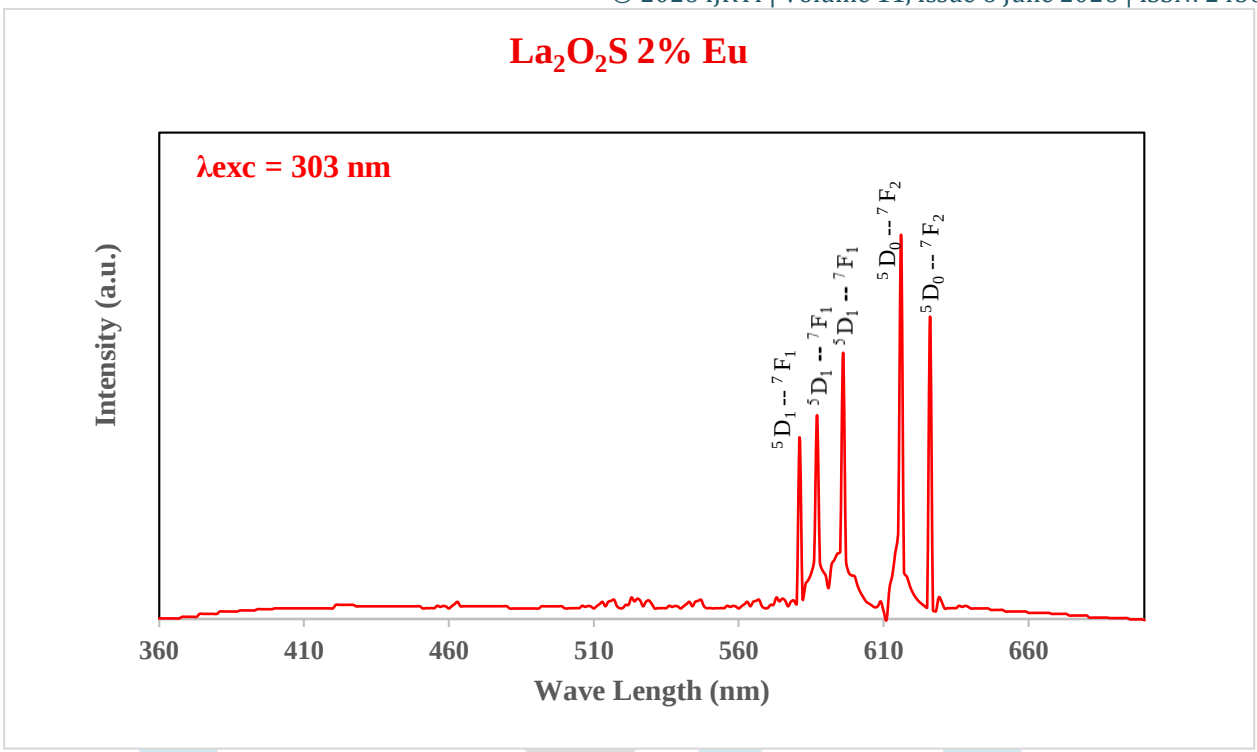

Fig. 13: Emission spectra of $La_2O_2S:Eu^{3+}$

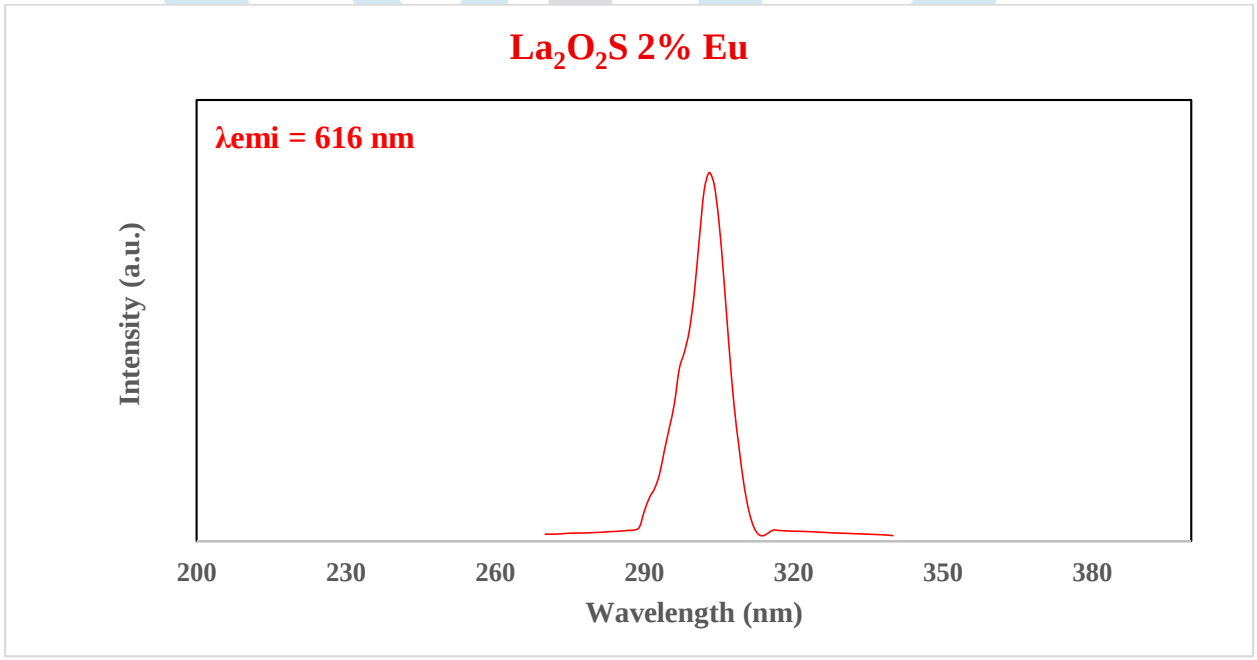

Fig. 14: Excitation spectra of $La_2O_2S:Eu^{3+}$

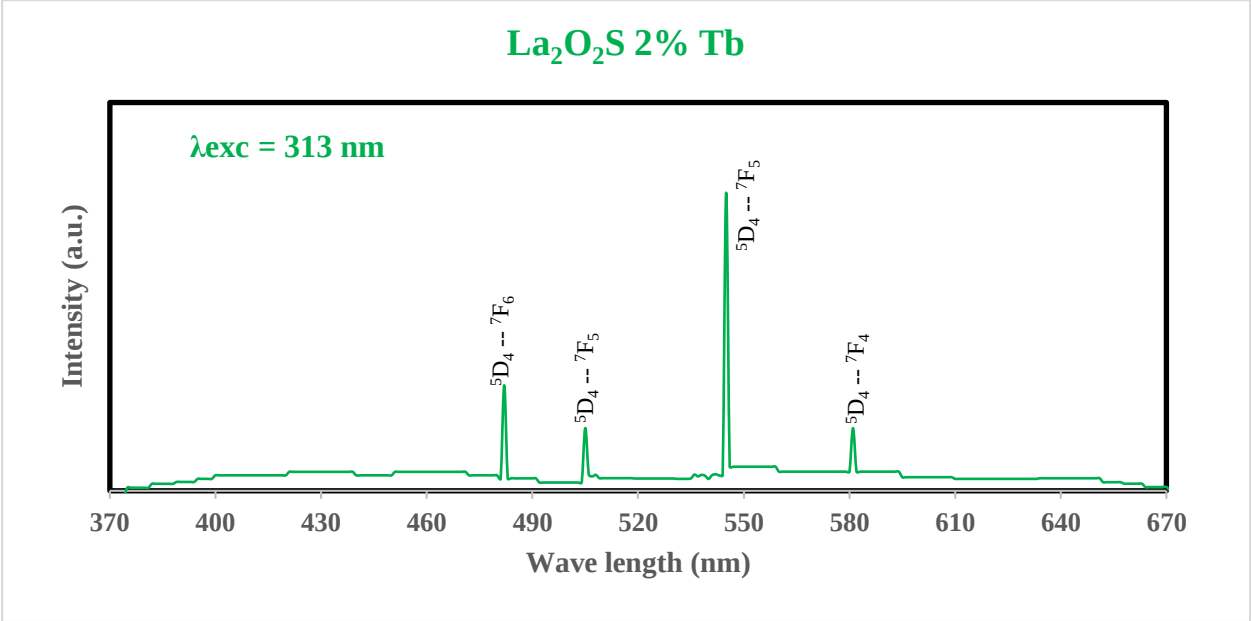

Fig. 15: Emission spectra of $La_2O_2S:Tb^{3+}$

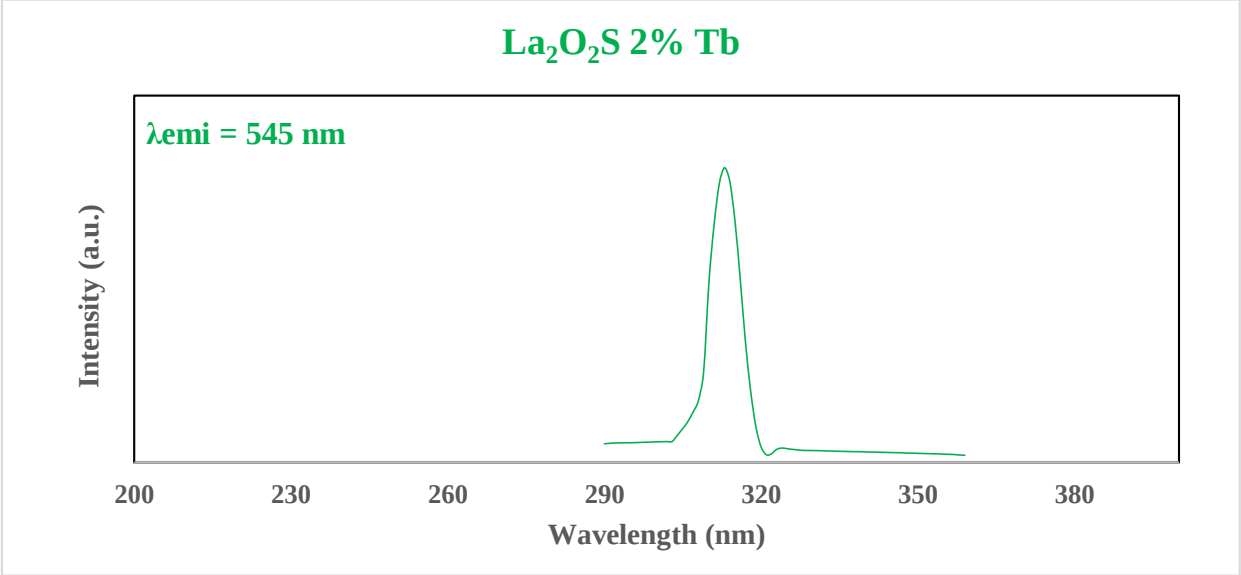

Fig. 16: Excitation spectra of $La_2O_2S:Tb^{3+}$

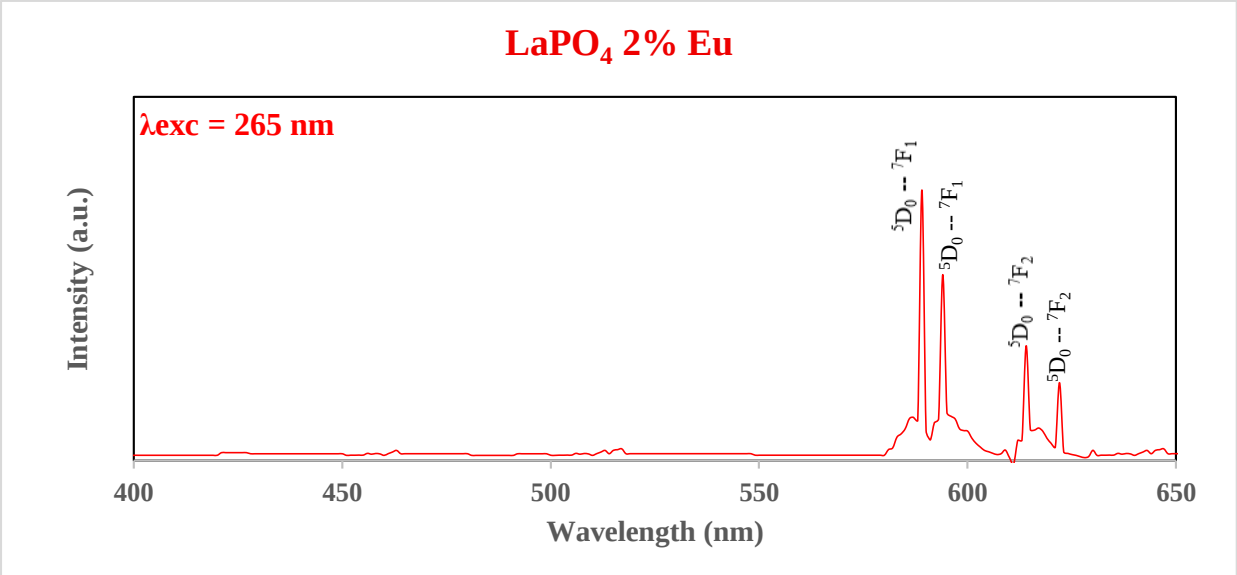

Fig. 17: Emission spectra of $LaPO_4:Eu^{3+}$

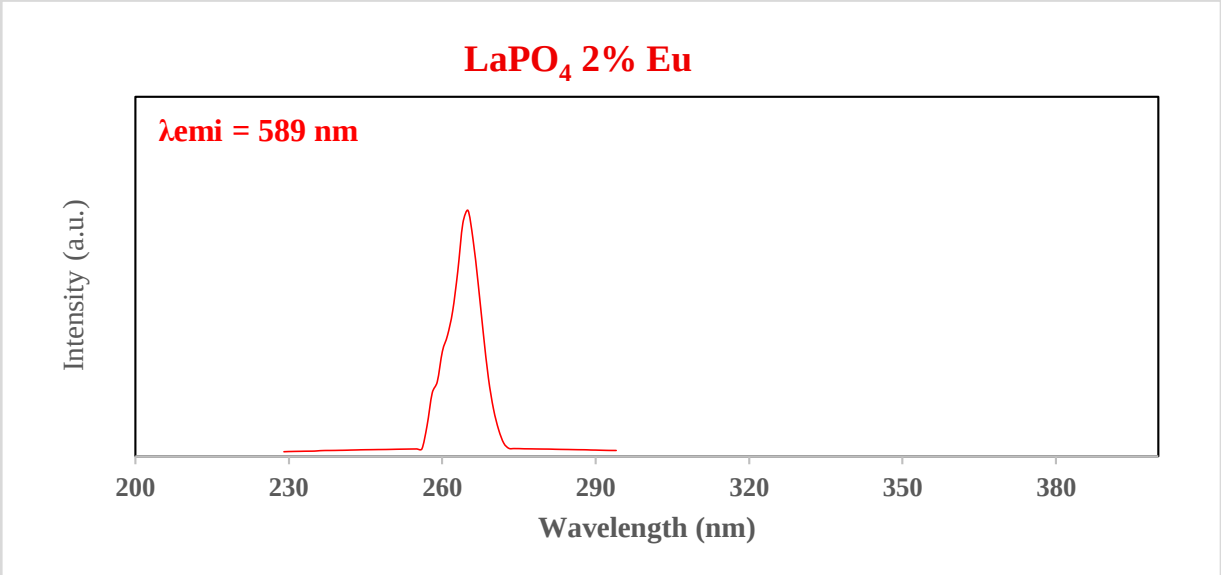

Fig. 18: Excitation spectra of $LaPO_4:Eu^{3+}$

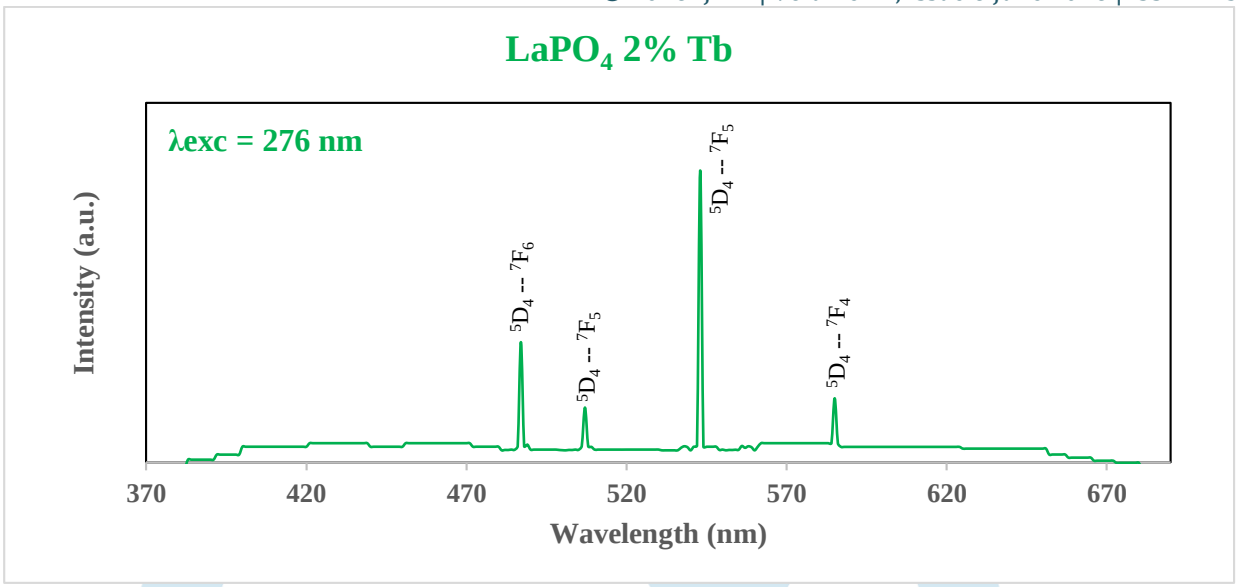

Fig. 19: Emission spectra of $LaPO_4:Tb^{3+}$

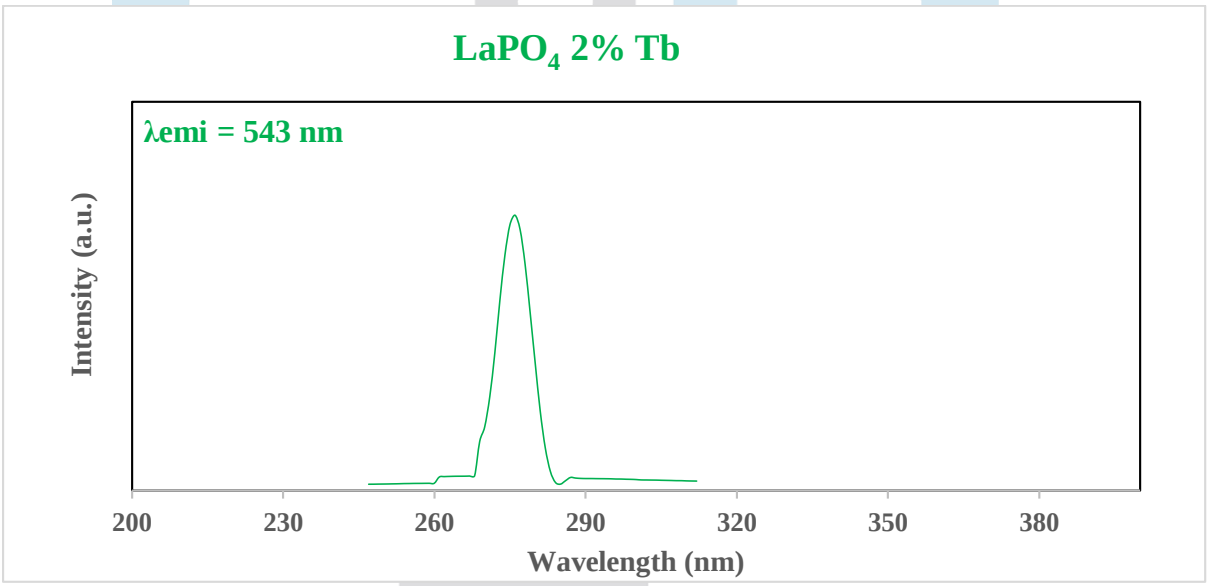

Fig. 20: Excitation spectra of $LaPO_4:Tb^{3+}$

Generally, efficient photoluminescence is observed in rare earth phosphors, which are crystalline compounds with rare-earth cations forming the host lattices. In most of these host lattices, inert rare earth activator cations can be substitutionally incorporated due to their close similarity in crystal structure, ionic size and iconicity. It is due to this substitutional incorporation that large atomic percentage of activator ions can be incorporated in a rare earth host lattice in place of the inert rare earth ions. The inert rare earth hosts do not interfere with the emission behaviour of the activators. Some of these rare earth phosphors can withstand very high excitation densities without exhibiting saturation behaviour.

In Lanthanum compounds, the dopant ions like Eu^{3+} (Red) and Tb^{3+} (Green) replace La^{3+} ions in the crystal lattice. The trivalent dopants $Eu^{3+}$and Tb^{3+} show distinct transitions due to their 4f electronic configurations. These transitions between specific quantum states called term symbols describe the movement of electrons between them during excitation and emission and are given by the energy level diagram referred to as Dieke Diagram.

Both Eu^{3+} and Tb^{3+} give multiple peaks in orange-red and blue green –green-orange region respectively. The number of peaks is higher in case of Eu^{3+}. There is variation in the relative intensities of the peaks, particularly in Eu^{3+}, as shown in figure. The peak with maximum intensity varies with the host matrix from orange to red. While the most intense peak in La_2O_3 is in the red region at 624nm, in La_2O_2S it is also in red region at 617 nm and shifts further to orange at 590 nm in $LaPO_4$.

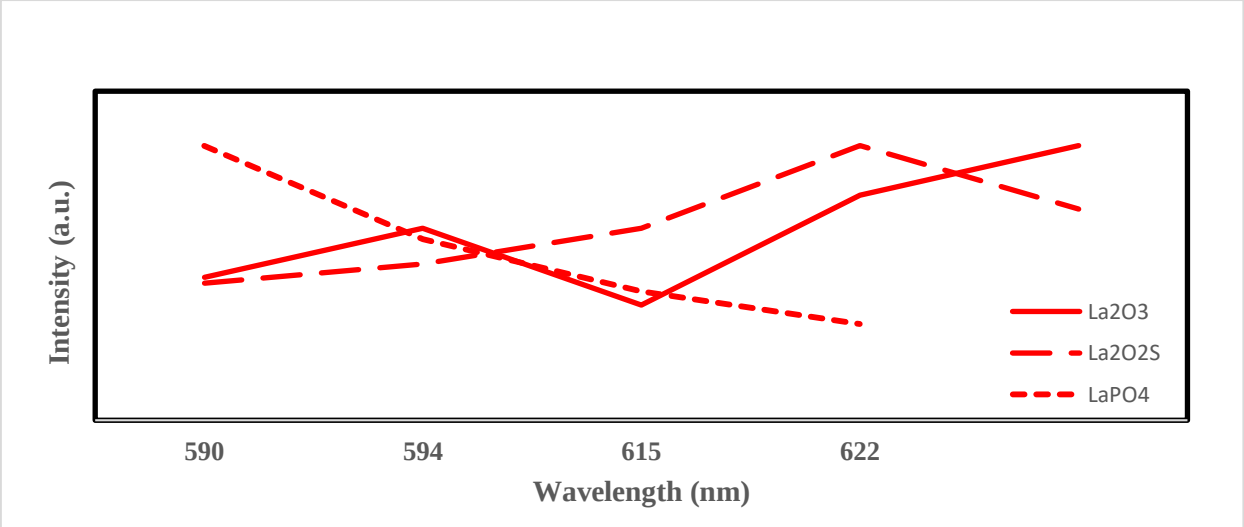

Fig. 21: Variation in the intensity of Eu $^{3+}$ peaks

$Eu^{3+}$is a prototypical red-emitting ion and retains its emission properties in the phosphor. The host does not have a profound effect on these ions, although there might be some difference between the emission features of Eu^{3+} in different host materials, due to reasons like site symmetry of the dopant ions and energy transfer mechanisms. The site symmetry is heavily dependent on the crystal structure. This significantly influences the intensity of certain emission lines.

The Eu^{3+} ion generally gives its characteristic emission in the orange - red region with a number of narrow lines due to the 4f-4f ($^5D_0$- ^7F_J = 0,1,2,3,4) transitions [27]. The luminescence spectrum of Eu^{3+} ion is slightly influenced by surrounding ligands of the host material because electronic transitions Eu^{3+} involve only a redistribution of electrons within the inner 4f sub-shell. Ultraviolet radiation is efficiently absorbed by a transition to the charge transfer state (CTS) of the $Eu^{3+} – O^{2-}$. After non-radiative relaxation to the lower 4f levels, luminescence occurs from the ^5D_J (mainly $^5D_0$) states of Eu^{3+}.

The shape of the emission spectra and emission peak wavelength is independent of the excitation wavelengths. The emission spectra monitored at the most intense Eu^{3+} emission wavelength is in agreement with those previously reported for the Eu-doped systems [28], indicating that Eu3+ ions have been adequately doped into the host lattice.

In general, the emission transitions include $^5D_0 \rightarrow {}^7F_0$ around 578.3nm, $^5D_0 \rightarrow {}^7F_1$ at (587–594 nm), $^5D_0 \rightarrow {}^7F_2$ at (611–620 nm), $^5D_0 \rightarrow {}^7F_3$ at (648–652 nm) and $^5D_0 \rightarrow {}^7F_4$ at (685–698 nm). Among them, the $^5D_0 \rightarrow {}^7F_1$ transitions are characterized by an orange–red emission. The $^5D_0 \rightarrow {}^7F_1$ lines originate from the magnetic dipole transition, while the $^5D_0 \rightarrow {}^7F_2$ lines characterized by red emission and originate from the electric dipole transition. The electric dipole transition is allowed exceptionally on the condition that the europium ion occupies a site without an inversion centre and is sensitive to local symmetry. Due to the magnetic dipole transitions $^5D_0 \rightarrow {}^7F_1$ and electric dipole transitions $^5D_0 \rightarrow {}^7F_2$ this phosphor gives emission over the orange-red region.

Due to the little difference between ionic sizes of Eu^{3+} ion and La^{3+} ion, the Eu^{3+} ions can occupy La^{3+} ion sites (C1 symmetry), which gives rise to a characteristic crystal splitting of the energy levels. The transitions are found to be split into components depending upon the host matrix composition. Due to the dependency between $^5D_0 \rightarrow {}^7F_1$ emissions and the crystal field, the $^7F_1$ level, which is associated with the site symmetry, can split into three Stark lines in the crystal field and the $^5D_0 \rightarrow {}^7F_2$ transition of Eu^{3+} can split into, at most, five lines in the crystal field.

To further elaborate on the dependence of emission peaks on site symmetry of the dopant ions and energy transfer mechanisms, the illustration of $LaPO_4$ will be appropriate. $LaPO_4$ typically crystallizes in the monazite structure (monoclinic), where the dopant site has low symmetry C_1. Consequently, the $^5D_0 \rightarrow {}^7F_1$ transition is relatively strong when the Eu^{3+} ions occupy inversion center sites, while the $^5D_0 \rightarrow {}^7F_2$ transition must be relatively weak due to the localized energy transfer. Hence, in the emission spectra, the peaks are positioned around 590 nm. These peaks correspond to the magnetic dipole transitions $^5D_0 \rightarrow {}^7F_1$ and are much stronger than the 614 and 622 nm ($^5D_0 \rightarrow {}^7F_2$) emission. Therefore, it can be inferred that the Eu^{3+} ions in $LaPO_4$ are located at a site with inversion symmetry.

In the emission characteristics of Tb^{3+}, the most prominent peak is around 545 nm, which is the characteristic green emission by Tb^{3+} ions. In addition to this, there are other peaks around 490 nm, 510 nm and 580 nm. These peaks are also associated with Tb^{3+} ions. The emission line in the green region lying at 545 nm is due to the $^5D_4 \rightarrow {}^7F_6$ transition. The peak around 580 nm in the orange region is due to $^5D_4 \rightarrow {}^7F_4$ and around 490 nm as well as 510 nm in the blue-green region due to $^5D_4 \rightarrow {}^7F_J$ transitions. There are in fact multiple emission lines at each transition due to the crystal field splitting of the ground state of the emitting ions. All the four emission lines, typical of Tb^{3+} doped phosphors are related to magnetic dipole transitions within 4f shell of Tb^{3+} ions.

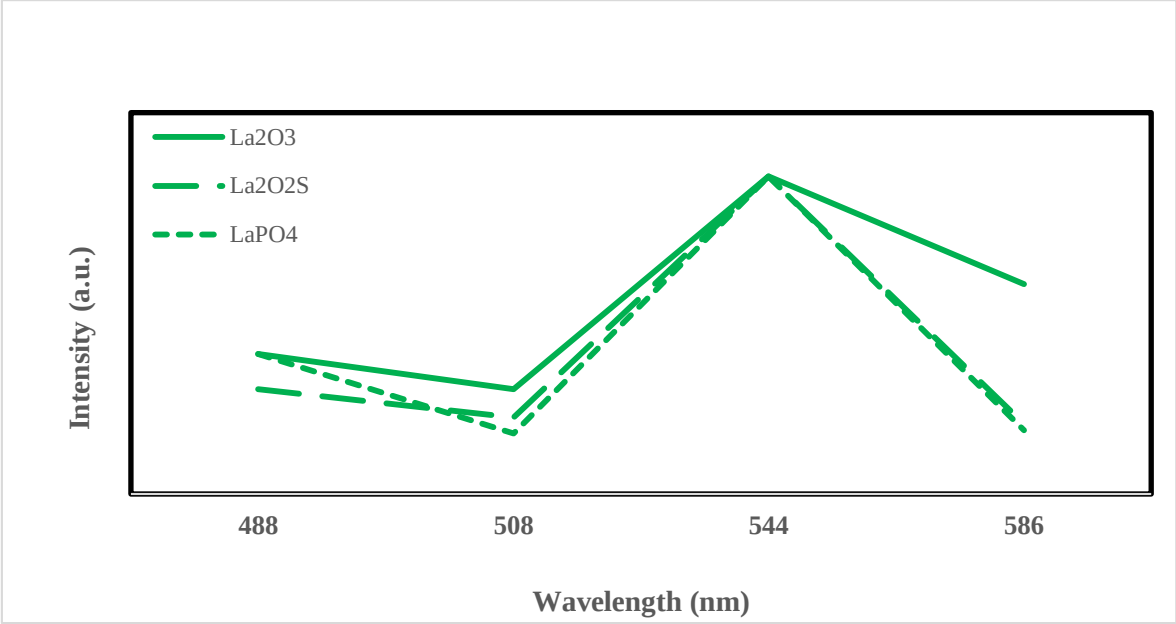

Fig.22: Variation in the intensity of Tb $^{3+}$ peaks

There is minimal variation in the relative intensities of the peaks, as shown in fig. 8. However, unlike Eu^{3+}, the peak with maximum intensity does not vary and remains around 545 nm in all the host materials. Other peaks also do not show much variation.

As stated earlier, due to the shielding of electrons in Tb^{3+} ions, there is no apparent effect on the emission characteristics of these ions due to the crystal field. Hence, Tb^{3+} ions show the same emission characteristics in different host lattices like aluminates, borates, silicates and oxysulphides. In the trivalent rare earth ions, the luminescence arises mainly due to transitions within the 4f shell. The efficiency of emission depends on the number of electrons in the 4f shell. The Tb^{3+} ion has 8 electrons in the 4f shell, which can be excited in the 4f-5d excitation band. The electron in the excited $^4f_7 \rightarrow$ 5d state remains at the surface of the ion and comes under the strong influence of the crystal field resulting in the splitting of the excitation band, giving broad band excitation spectra. The excited ion in the $^4F_7 \rightarrow$ 5D level decays stepwise from this state to the luminescent levels $^5D_3$ or $^5D_4$ by giving up phonons to the lattice. Luminescence emission occurs from either of these states, thereby the ion returning to the ground state. For display

applications, particularly televisions, it is preferable to have a single peak at 545 nm to obtain good color purity.

4 References

1. Maury, O., & Murugesu, M. *Lanthanide Photonics: Shaping the Nanoworld*. Trends in Chemistry, 1(8), 751–762 (2019). https://doi.org/10.1016/j.trechm.2019.05.012.
2. Bünzli, J.-C. G., & Eliseeva, S. V. *Lanthanide luminescence for functional materials and bio-sciences*. Chemical Society Reviews, 39(1), 189–227 (2010). https://doi.org/10.1039/B905604C.
3. Bünzli, J.-C. G., & Piguet, C. (2005). *Taking advantage of luminescent lanthanide ions*. Chemical Society Reviews, 34(12), 1048–1077. https://doi.org/10.1039/B406082M.
4. Blasse, G., & Grabmaier, B. C. (1994). *Luminescent Materials*. Springer-Verlag, Berlin. https://doi.org/10.1007/978-3-642-79017-1.
5. Auzel, F. (2004). *Upconversion and Anti-Stokes Processes with f and d Ions in Solids*. Chemical Reviews, 104(1), 139–174. https://doi.org/10.1021/cr020357g.
6. Eliseeva, S. V., & Bünzli, J.-C. G. (2010). *Rare earths: jewels for functional materials of the future*. New Journal of Chemistry, 35(6), 1165–1176. https://doi.org/10.1039/C0NJ00969E.
7. Dorenbos, P. (2003). Energy of the first 4f–5d transition of Ce^{3+} in inorganic compounds. *Journal of Luminescence, 104*(4), 239–260. https://doi.org/10.1016/S0022-2313(03)00078-4.
8. Binnemans, K. (2015). Interpretation of europium (III) spectra. *Coordination Chemistry Reviews, 295*, 1–45. https://doi.org/10.1016/j.ccr.2015.02.015.
9. Dorenbos, P. (2005). The 5d level positions of the trivalent lanthanides in inorganic compounds. *Journal of Luminescence, 111*(1–2), 89–104. https://doi.org/10.1016/j.jlumin.2004.07.006.
10. Boatner, L. A., & Sales, B. C. (1988). Monazite. In *Reviews in Mineralogy* (Vol. 21, pp. 495–564). Mineralogical Society of America.
11. Kumar, S., Singh, R., & Kumar, A. (2021). Structural, optical, and thermal properties of lanthanum phosphate ($LaPO_4$). *Solid State Communications, 335*, 114421. https://doi.org/10.1016/j.ssc.2021.114421
12. Zhang, Y., Liu, X., Li, J., & Wang, H. (2018). First-principles study on structural stability and electronic properties of rare-earth phosphates $LaPO_4$. *Materials Science and Engineering: B, 229*, 1–6. https://doi.org/10.1016/j.mseb.2017.12.012
13. Shravani S. More, S. S. M., Sandhya P. Kadam, S. P. K., & Dr. Vivekkumar K. Redasani, Dr. V. K. R. (2025b). A Comprehensive Review of UV-visible spectroscopy. International Journal of Pharmaceutical Research and Applications, 10(3), 114–134. https://doi.org/10.35629/4494-1003114134.

14. Blasse, G., & Grabmaier, B. C. (1994). *Luminescent materials*. Springer. https://doi.org/10.1007/978-3-540-57819-1.
15. Sheikh Wajiha Shabbir, & Shilpi Chauhan. (2024). A REVIEW ON USE OF ULTRAVIOLET SPECTROSCOPY. Innovare Journal of Medical Sciences, 5–11. https://doi.org/10.22159/ijms.2024v12i4.51499.
16. Carnall, W. T., Fields, P. R., & Rajnak, K. (1989). Electronic energy levels in the trivalent lanthanide aquo ions. *Journal of Chemical Physics*, *90*(7), 3443–3457. https://doi.org/10.1063/1.455853.
17. Henderson, B., & Imbusch, G. F. (1989). Optical spectroscopy of inorganic solids. Oxford University Press. https://doi.org/10.1093/acprof:oso/9780198552948.001.0001.
18. Eliseeva, S. V., & Bünzli, J.-C. G. (2010). Lanthanide luminescence for functional materials and bio-sciences. Chemical Society Reviews, 39(1), 189–227. https://doi.org/10.1039/B905604C
19. Yu, P. Y., & Cardona, M. (2010). *Fundamentals of semiconductors: Physics and materials properties* (4th ed.). Springer. https://doi.org/10.1007/978-3-642-00710-1.
20. Fox, M. (2010). *Optical properties of solids* (2nd ed.). Oxford University Press. https://doi.org/10.1093/acprof:oso/9780199573379.001.0001.
21. Urbach, F. (1953). The long-wavelength edge of photographic sensitivity and of the electronic absorption of solids. *Physical Review*, *92*(5), 1324. https://doi.org/10.1103/PhysRev.92.1324.
22. Cody, G. D., Tiedje, T., Abeles, B., Brooks, B., & Goldstein, Y. (1981). Disorder and the optical-absorption edge of hydrogenated amorphous silicon. *Physical Review Letters*, *47*(20), 1480–1483. https://doi.org/10.1103/PhysRevLett.47.1480.
23. Van de Walle, C. G., & Neugebauer, J. (2004). First-principles calculations for defects and impurities: Applications to III-nitrides. *Journal of Applied Physics*, *95*(8), 3851–3879. https://doi.org/10.1063/1.1682673
24. Tauc, J., Grigorovici, R., & Vancu, A. (1966). Optical properties and electronic structure of amorphous germanium. *Physica Status Solidi (b)*, *15*(2), 627–637. https://doi.org/10.1002/pssb.19660150224.
25. Paithane, P. R., Gore, K. R., Waghmare, S., & Kamble, D. H. (2024a). A Review on Uv-Visible Spectroscopy. 11.
26. Mäntele, W., & Deniz, E. (2017). *UV-VIS absorption spectroscopy: Lambert-Beer reloaded*. **Spectrochimica Acta Part A: Molecular and Biomolecular Spectroscopy, 173**, 965–968. https://doi.org/10.1016/j.saa.2016.09.037
27. Binnemans, K. (2015). *Interpretation of europium(III) spectra*. **Coordination Chemistry Reviews, 295**, 1–45. https://doi.org/10.1016/j.ccr.2015.02.015
28. Reisfeld, R., & Jørgensen, C. K. (1977). *Lasers and Excited States of Rare Earths*. Springer. https://doi.org/10.1007/978-3-642-66698-8